NRAP
National Risk Assessment Partnership

Compressive and Tensile Strength of Class H Cement Exposed to High Pressure and Temperature Storage Conditions

28 March 2017

U.S. DEPARTMENT OF ENERGY | NATIONAL ENERGY TECHNOLOGY LABORATORY

Office of Fossil Energy

NRAP-TRS-III-004-2017

Disclaimer

Cover Illustration: Scanning electron microscopy (SEM) montage image of the fresh *surrogate* cement paste sample after 84 days immersed in CO_2-saturated brine which displays alteration around the outer rim of the cement cylinder (outlined by white dotted line).

Suggested Citation: Verba, C.; Reed, M.; Ideker, J.; O'Connor, W. *Compressive and Tensile Strength of Class H Cement Exposed to High Pressure and Temperature Storage Conditions*; NRAP-TRS-III-004-2017; NRAP Technical Report Series; U.S. Department of Energy, National Energy Technology Laboratory: Albany, OR, 2017; p 32.

An electronic version of this report can be found at:
http://www.netl.doe.gov/research/on-site-research/publications/featured-technical-reports

https://edx.netl.doe.gov/nrap

Compressive and Tensile Strength of Class H Cement Exposed to High Pressure and Temperature Storage Conditions

Circe Verba[1], Mark Reed[2], Jason Ideker[3], William O'Connor[1]

[1] U. S. Department of Energy, Office of Research and Development, National Energy Technology Laboratory, 1450 SW Queen Avenue, Albany, OR 97321

[2]University of Oregon, 1585 E 13th Avenue, Eugene, OR 97403

[3]College of Engineering, Oregon State University, 101 Covell Hall, Corvallis, OR 97331

NRAP-TRS-III-004-2017

Level III Technical Report Series

28 March 2017

This page intentionally left blank.

Table of Contents

List of Figures

List of Tables

Acronyms, Abbreviations, and Symbols

Term	Description
API	American Petroleum Institute
ASTM	American Standard for Testing and Materials
BSE	Backscatter electron
CO_2	Carbon dioxide
C-S-H	Calcium-silicate-hydrate
DOE	U.S. Department of Energy
EDS	Energy dispersive spectroscopy
EOR	Enhanced oil recovery
EPA	U.S. Environmental Protection Agency
ICDD	International Center for Diffraction Data
LOI	Loss on ignition
NETL	National Energy Technology Laboratory
NRAP	National Risk Assessment Partnership
OPC	Ordinary Portland cement
SEM	Scanning electron microscopy
sCO_2	Supercritical CO_2
SO_2	Sulfur-dioxide
TDS	Total dissolved solids
UIC	Underground Injection Control
XRD	X-ray diffraction
w/c	Water-cement

Acknowledgments

This work was completed as part of the National Risk Assessment Partnership (NRAP) project. Support for this project came from the U.S. Department of Energy's (DOE) Office of Fossil Energy's Crosscutting Research program. The authors wish to acknowledge Traci Rodosta (Carbon Storage Technology Manager), Kanwal Mahajan (Carbon Storage Division Director), M. Kylee Rice (Carbon Storage Division Project Manager), Mark Ackiewicz (Division of CCS Research Program Manager), Darin Damiani (Carbon Storage Program Manager), Robert Romanosky (NETL Crosscutting Research, Office of Strategic Planning), and Regis Conrad (DOE Office of Fossil Energy) for programmatic guidance, direction, and support.

Special thanks go to the NETL Seal Integrity team, Barbara Kutchko, Deborah Glosser, Gilbert Rush, and John Logan for contributions. The authors also thank the reviewers for their comments and recommendations.

ABSTRACT

In the United States, the implementation of [co]-storage (CO_2-O_2-SO_2 mixtures) from oxy-fueled combustion, coal gasification and sour gas is currently being considered in saline geologic formations. The U.S. Department of Energy's (DOE) National Energy Technology Laboratory (NETL), as part of the National Risk Assessment Partnership (NRAP), was tasked to determine the risk related to geologic carbon storage. This report addresses the potential impacts on wellbore cement integrity following exposure to storage conditions. When plumes of injected CO_2 (or co-stored) gas come in contact with existing wells, the cement lining in the well is vulnerable to geochemical alteration, and impact the well's effectiveness as a barrier for unwanted fluid migration. In this study, cured Class H cement paste, used in well construction, was exposed to co-storage conditions, and the tensile and compressive strength were measured to understand the effects of co-stored gas on the geomechanical properties of cement. In addition, co-storage settings at higher formation temperatures may result in loss of cement strength under acidic conditions, though cement integrity has not been tested under fully in situ conditions. These observed effects have implications for the long-term effectiveness of wells using Class H cement paste in co-storage scenarios.

1. INTRODUCTION

1.1 CO_2 STORAGE AND CHALLENGES

This study is a cross-cutting effort to aid in the safe and permanent storage of carbon dioxide (CO_2) under the National Risk Assessment Partnership (NRAP), an initiative within the U.S. Department of Energy (DOE), Office of Fossil Energy's Carbon Capture and Storage Program at the National Energy Technology Laboratory (NETL). The intention of this study was to identify changes in wellbore cement after exposure to co-storage gases dissolved in fluid by measuring cement paste physical strength. The compressive and tensile strength of Class H cement was examined after exposure to pure-CO_2, CO_2-O_2-mixture, and CO_2-O_2-H_2SO_4 co-storage environments. Geomechanical properties of Class H Portland cement subjected to selected co-storage conditions were determined using both compressive and tensile strength tests. The experimental conditions used in this study are based on Regional Carbon Storage Partnership Phase II injection sites, which typically occur at depths from 2.29–3.35 km, pressures from 24.1–32.0 MPa, and temperatures from 69–125°C (NATCARB, 2013).

Large quantities of CO_2, a greenhouse gas, are emitted as a result of utilization of fossil energy resources, such as coal combustion for thermoelectric generation. Injection and geologic storage of CO_2 in the subsurface is being considered to mitigate the accumulation of CO_2 in the atmosphere. Brine-bearing geologic formations are the largest volume potential target for long-term (>1,000 years) geologic storage of CO_2 (e.g. Bergman and Winter, 1995; Bruant et al., 2002; DOE, 2015). An ideal deep saline storage formation candidate will have sufficient permeability and porosity to store large-quantities of CO_2. The U.S. Environmental Protection Agency (EPA) Underground Injection Control (UIC) program mandates that this brine greater than 10,000 total dissolved solids (TDS) to avoid being considered as an underground source of drinking water (Goodman et al., 2011). Such a formation will be overlain by an impermeable caprock, typically shale, to prevent leakage or contamination into overlying receptors of concern (including freshwater aquifers and the atmosphere) (Figure 1).

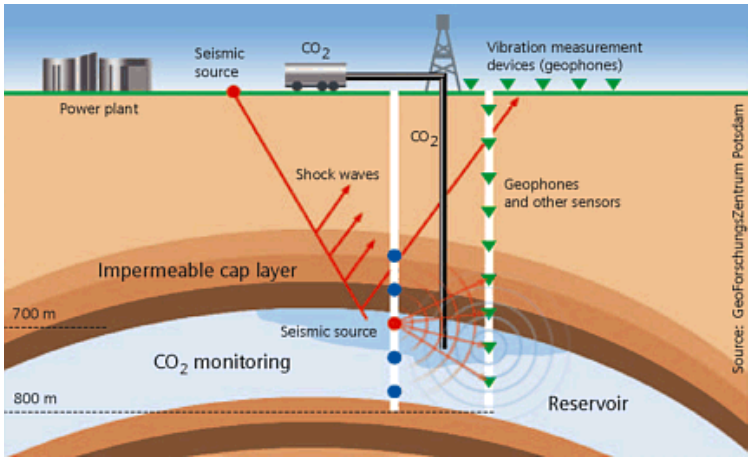

Figure 1: Geologic storage from CO_2 production to CO_2 injection into a reservoir with a caprock (DOE, 2007).

It is known that supercritical CO_2 (sCO_2) will alter wellbore cement (as reviewed by Zhang and Bachu, 2011), and the integrity of the wellbore seal is of concern because wellbores are the primary potential engineered pathway for unwanted vertical migration of CO_2. Wellbore cement

is a critical component for the creation and preservation of zonal isolation, and alteration of wellbore cement can present potential risks for seal integrity. For instance, leakage could occur between the cement and the steel casing or the formation rock (Duguid and Scherer, 2009; Rimmelé et al., 2008). In cases where CO_2 dissolves into the brine, carbonic acid (H_2CO_3) is generated and subsequently interacts with the cement. Previous studies have found that wellbore cement exposed to pure supercritical CO_2 and CO_2-saturated brine at simulated downhole conditions result in cement alteration and calcium carbonate precipitation (e.g. Duiguid et al., 2005; Barlet-Gouédard et al., 2009; Kutchko et al., 2007, 2008, 2009). The extent of the alteration over decadal time scales has been modeled in previous work. Kutchko et al. (2008) conducted a study in which Class H cement was exposed to CO_2-saturated brine for up to 1 year. Monte Carlo and Elovich diffusion modeling showed that alteration depth extrapolates to ~1 mm after 20 years of exposure to CO_2. Prior work has also tied CO_2 used for enhanced oil recovery (EOR) to losses in wellbore integrity in the field. Bachu and Watson (2009) studied 79 wells in Alberta, Canada where CO_2 was used for EOR operations and acid gas (H_2S and CO_2 mixture). In all cases according to the authors, converted wells failed at higher rates than wells specifically used for injection.

1.2 CEMENT BACKGROUND

To understand the mechanisms of cement alteration under $SCCO_2$ conditions, it is important to characterize its initial chemistry. The major components of Portland cement are tricalcium silicate (Ca_3SiO_5), dicalcium silicate (Ca_2SiO_3), tricalcium aluminate ($Ca_3Al_2O_6$), and calcium aluminoferrite (Ca_4AlFeO_5). Gypsum ($CaSO_4 \cdot 2H_2O$) is added and integrated with the clinker to prevent instantaneous flash set. Hydration products form when the components of Portland cement are mixed with water. The primary hydration products of Portland cement form a network of a semi-amorphous gel, calcium-silicate-hydrate ($Ca_xSi_x*xH_2O$, abbreviated cement nomenclature as C-S-H) and Portlandite, or calcium hydroxide ($Ca(OH)_2$) (Reactions 1 and 2 below). The hydration reactions from Nelson (1990) in oxide notation are as follows:

$$2Ca_3SiO_5 + 6H \rightarrow Ca_3Si_2 \cdot 3H_2O + 3Ca(OH)_2 \quad (1)$$

$$2Ca_2SiO_3 + 4H \rightarrow Ca_3Si_2 \cdot 3H_2O + Ca(OH)_2 \quad (2)$$

Other hydration products include lesser amounts of ettringite ($Ca_6Al_2(SO_4)_3(OH)_{12} \cdot 26H_2O$) or monosulfoaluminate hydrate (often referred to as monosulfate) are present as a result of tricalcium aluminate hydration in most cement types. Minor amounts of amorphous iron (III) oxy-hydroxides [FeOOH] or hydroxide [$Fe(OH)_3$] are present from calcium aluminoferrite hydration (Glasser et al., 2008; Taylor, 1997). Understanding these cement phases is essential to interpreting CO_2 related reactions.

In situ wellbore cement is exposed to time and depth dependent variations in pressure and temperature. Pressure and temperature influence the hydration process and can ultimately influence the hydration products as well (Hewlet, 1998), which can in turn influence cement alteration, structure, and mechanical strength of the cured cement. Hydration temperature is a particularly important factor in the stability and morphology of the mineral products. Increasing

the temperature (T > 23°C) increases the initial rate of hydration, thereby affecting the microstructure and ultimately reduces the overall long-term strength of the cement paste. As temperatures increase to >40°C, C-S-H becomes more fibrous and crystalline, and the hydrate ultimately becomes unstable above 110°C (Le Saout et al., 2004; Nelson, 1990). At temperatures above 160°C or pressures above 34.47 MPa, the C-S-H structure polymerizes into a crystalline structure with increased silicate chain such as tobermorite or jaffeite (Bresson et al., 2002; Bresson and Zanni, 1998). Although pressure alone does not greatly affect cement hydration, it is an important contributor in combination with increasing temperatures during the curing process.

1.3 CARBONATION OF CEMENT

As described above, C-S-H and $Ca(OH)_2$ are the primary hydration products in Portland cement. Calcium hydroxide is stable at pH of 12–13, whereas C-S-H is stable at a pH of ~10–11 (Lecolier et al., 2006). As CO_2 comes into contact with the formation fluid it will yield carbonic acid at a pH of ~2–4. This carbonic acid will react with the cement as outlined by Kutchko et al. (2007) and demonstrated in Figure 2.

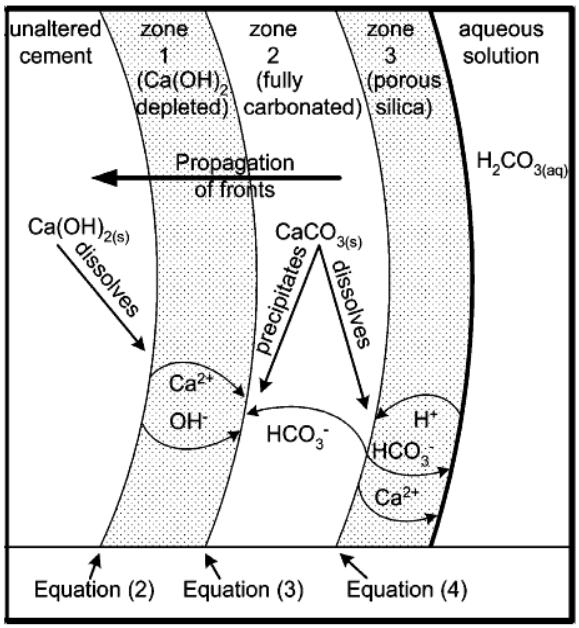

Figure 2: Schematic displaying calcium migration and dissolution in the formation of alteration fronts (from Kutchko et al., 2007).

The impact of continuous exposure to carbonic fluid on the cement strength is not well understood. However, the precipitation of $CaCO_3$ initially increases the cement's compressive strength and reduces its permeability. Nevertheless, microfractures may form in the carbonated zone due to volume expansion (Johannesson and Utgenannt, 2001). It is not certain if expansion will occur under the confined stress conditions found within the wellbore as it does in atmospheric conditions. The continuous contact of the cement with carbonic acid will eventually cause $CaCO_3$ to dissolve and lead to cement degradation. As the $CaCO_3$ becomes increasingly unstable, carbonated fluid begins to diffuse inward and Ca^{2+} ions diffuse outward into solution. As the dissolution of the C-S-H takes effect, an amorphous silica gel is formed and the cement

volume decreases, which in turn increases cement permeability (Shen, 1989). The diffusion either stabilizes in a static system, or the cement continues to degrade with continued injection of CO_2 (Zhang and Bachu, 2011). Recent work by Hangx and van der Linden (2016) has shown depth dependent heterogeneities in cement alteration and mechanical structure. Here, cement was exposed to CO_2 rich fluids for one to six months at 65^{o}C and 8 MPa; brittleness and compressive strength tests were performed, and several distinct zones within the cement were identified based on the extent of the cement reactions. The changes in cement mechanics were found to be only loosely related to exposure time (Hangx and van der Linden, 2016).

1.4 PRECIPITATION OF EXPANSIVE MINERALS IN CEMENT

As described previously, cement expansion can lead to microfracturing and the potential for the creation of pathways for fluid flow through the cement matrix (Walsh et al., 2014). Precipitation of expansive minerals within the matrix of the hardened cement—often referred to as secondary mineral precipitation—is a concern with cement exposed to co-storage gases dissolved in formation fluids. The formation of carbonate minerals and ettringite has been observed in previous co-storage studies (Jacquemet et al., 2008; Moroni et al., 2008; Kutchko et al., 2011; Verba et al., 2012a; Verba et al., 2012b; Um and Rod, 2016). Ettringite can form when calcium and sulfate ions react with the aluminate and hydroxyl ions from the unhydrated $Ca_3Al_2O_6$ (Taylor et al., 2001). In addition to the minor amounts of ettringite that naturally occur in cement, external sources of sulfate ions can ingress into the cement matrix, and react with the calcium compounds to form secondary ettringite. This “secondary ettringite formation” is known to be responsible for cement and concrete degradation under atmospheric conditions (i.e. bridges and foundations in the construction industry) (Glasser, 2001). Precipitation of expansive minerals, such as ettringite, in the hardened cement may increase confined crystallization pressure in the cement pores and cause spalling or fracturing (Flatt and Scherer, 2008). Studies from Johansen et al. (1993) and Taylor (2001) suggest that as expansion occurs, opportunistic ettringite and $Ca(OH)_2$ will precipitate in the resulting fractures. The extent to which secondary ettringite is responsible for cement degradation under wellbore conditions is unknown.

Both temperature and the pH of the cement pore solution play an important role in ettringite formation. Stark and Bollard (1999) compared data published on the stability of ettringite and concluded that the mineral is found where the local pH ranges from 9 to 13.4. For example, Verba et al. (2012a) initially identified ettringite in cement after exposure to CO_2-O_2 conditions at environmental temperatures of 50°C and 85°C. These initial studies by Verba et al. (2012a) demonstrate that cement exposed to only CO_2 did not result in any ettringite, whereas the addition of oxygen allowed for ettringite precipitation. Within the pore solution, dissolved CO_2 also lowers pH, which leaches sulfate from bound C-S-H. Thermal decomposition of ettringite or late sulfate released from C-S-H is an example of an internal sulfate attack. This sulfate ion release can result in damage in a sulfate-free environment (Diamond, 1996; Collepardi, 1999; 2003).

2. MATERIALS AND METHODS

2.1 CEMENT AND CO_2 CONDITIONS

The present study used cement samples composed of Class H Portland cement manufactured by Lafarge. The cement samples were mixed in a 1 M brine consisting of 0.16 mol/L $CaCl_2$, 0.02 mol/l $MgCl_2$, and 0.82 mol/l NaCl, to represent water that would be utilized directly at the drill site. A Bogue calculation was used to calculate approximate proportions of the primary minerals in a cement clinker. This calculation takes the total oxide content that was used to extrapolate the composition of the initial powder analysis of the cement (in weight percent). The majority of the cement is Ca_3SiO_5. The composition was 64.5% tricalcium silicate (Ca_3SiO_5), 11.77% dicalcium silicate (Ca_2SiO_3), 13.24% calcium aluminoferrite ($4CaO{\cdot}Al_2O_3{\cdot}Fe_2O_3$), 0% tricalcium aluminate ($Ca_3Al_2O_6$), 2.94% MgO, 2.8% SO_4^{2-}, 0.16% total alkali content (Na_2O), and 0.62% free lime. The total volatile material lost (water bound) calculated based on oxide analysis resulted in a loss on ignition (LOI) of 0.73. The samples had a water-cement (w/c) ratio of 0.38 based on practices recommended by the American Petroleum Institute (API) (API, 1997).

Cement slurry was mixed according to API Recommended Practice 10b and poured into 25 mm x 152 mm PVC-pipe forms and placed vertically into 1.2 L stainless steel (316 CrNiMo) static autoclave vessels filled with 600 mL of brine and cured for 28 days at a hydraulic pressure of 28.9 MPa and temperatures of 50°C or 85°C. Immediately after curing, CO_2 was used to displace air and purge the autoclaves; the autoclaves were then returned to test temperature and pressure conditions and injected with gaseous CO_2 (or mixed gas). After the desired exposure period, samples designated for strength tests were removed, cut into 25-cm slices using ethanol as cutting fluid, and stored in vacuum-sealed Mylar® bags.

2.2 SULFURIC ACID CONDITIONS

To imitate exposure to sulfur-dioxide (SO_2) dissolved in brine, a gas composition of 94.5% CO_2, 4% O_2, and 1.5% SO_2 was first examined using the geochemical model CHIM-XPT (see Appendix A; Reed and Palandri, 2013; Palandri, 2005). The addition of SO_2 [to the CO_2-O_2 stream] disproportionates to sulfuric acid; the amount of H_2SO_4 was determined, along with the formation of carbonic acid and excess of supercritical CO_2 and O_2 generated from this process. Due to the corrosive nature of SO_2 gas within the laboratory, 7% H_2SO_4 was used based on the total modeled acid in a 1 M brine solution as described above as a proxy to represent hydrated cement samples in mixed gas conditions. Cement strength was measured once the cement had been exposed to CO_2-O_2 conditions for 28 days and then (42 mL) sulfuric acid solution was injected into the system for an additional 7 days at room temperature and pressure.

2.3 SAMPLE ANALYSIS

The samples were examined using an FEI Inspect F Scanning Electron Microscope (SEM) to obtain backscattered electron images (BSE) and energy dispersive spectroscopy (EDS) data. The cementitious and alteration phases were identified using X-ray diffraction (XRD) collected by a Rigaku Ultima III with a 40KV/40mA Cu k-α source and a step speed of 1°/min over a scan angle 2θ of 5°-90° (Table 1). To control phases sensitive to desiccation, samples were removed from respective solution and a wet grid preparation and immediate analysis was conducted. The qualitative analysis of XRD data was performed using Jade v9.1.4 Plus software and the International Center for Diffraction Data (ICDD) pattern databases (ICDD, 2008). Parallel Beam

Optics, which provides excellent peak position accuracy, was used along with the Fixed Diffracted Beam Monochromator between the sample and detector to reduce false peaks in Fe fluorescence data errors.

2.4 STRENGTH APPLICATIONS

Tensile and compressive tests were conducted to determine whether carbonation and secondary ettringite formation are detrimental or beneficial to wellbore cement integrity. Quantifying the change in compressive strength could provide analytical data for any strength loss due to secondary mineral precipitation or acid attack.

American Standard for Testing and Materials (ASTM) Standard C496 is a standard test method for measuring tensile strength of concrete specimens (molded cylinders). Because no cement standards are available for measuring tensile strength as a point load, a point load test was utilized that hydraulically compresses the cement sample between two steel spheres until failure occurs to simulate the tensile strength. A pressure gauge (gauge load) measures the applied load and calculates the apparent tensile strength using the thickness and diameter of the cylindrical samples. The equivalent uniaxial tensile strength was determined by applying Nigel's correction (Logan, 1993).

Compressive strength was determined by applying an axially directed force to the point of deformation, and failure occurred at the limit of compressive strength when the cement was crushed. Cement strength was calculated by dividing the maximum load at failure by the load dispersed over the cross-sectional area. Strength tests from the ASTM were used for quality control and strength value comparison. To determine acceptable concrete and cement in-place strength, several testing parameters must be considered. The standards for measuring compressive strengths vary (cubic, prism, or cylindrical), which gives a variety of strength values. For example, ASTM C 349: Compressive Strength of Hydraulic Cement Mortars (Using Portions of Prisms Broken in Flexure) and ASTM C 873: the Standard Test Method for Compressive Strength of Concrete Cylinders Cast in Place in Cylindrical Molds were considered. Kim et al. (1998), using the latter method, found that 28-day-old cylindrical ordinary Portland cement (OPC) cement at 40°C with a w/c=0.35 and cured for 7 days had a compressive strength of 51.7 MPa. The compressive strengths determined in this study were comparable to those obtained using the methodology of Kim et al. (1998), ASTM C 109, ASTM C 873-94 and ASTM C 150, respectively.

To examine the potential changes to the cement under representative wellbore conditions, the cement cylinders were encased in heat-treated polyolefin shrink jacket to simulate semi-confined settings. The primary method to measure the physical change in the cylinders was to determine: 1) compressive strength of cement paste cylinders roughly 2.54 x 2.54 mm in size (1:1 size ratio), and 2) tensile strength on 1.27 x 2.54 mm (1:2 size ratio) cement prior and post-exposure to storage conditions. Three sample types were examined: 1) a marble sample for relative loads, as representative of natural cemented limestone that has undergone higher pressure and temperature conditions; 2) hydrated cement; and 3) hydrated cement exposed to different gas types to replicate (co)-storage conditions. The uniaxial compressive strength can be measured by calculating the load and stress at cement cylinder failure within the hydraulic press.

3. RESULTS AND DISCUSSION

The precipitation of expansive minerals may cause the cement to expand slightly during exposure (Glasser, 2001; Hewlett, 1998). In the present study, initial strength measurements are compared to determine the impact of secondary mineral precipitation. The newly precipitated minerals impact the structural integrity of the cement as determined by the compressive and tensile tests.

3.1 ETTRINGITE FROM CO_2-O_2 REACTIONS

In the CO_2-O_2 exposed cement paste samples, XRD showed an increase of total cement alteration of ettringite after exposure to supercritical storage gases as compared to unexposed cement (Verba et al., 2012a) in Table 1. Typically, ettringite does not precipitate because Class H Portland cement has little or no calcium-aluminate content and Al^{3+} is fairly immobile in Ca_4AlFeO_5. In addition, the only source of sulfur is from the original gypsum mixed in that was tied into the C-S-H structure during hydration.

Table 1: XRD analyses of CO_2 and CO_2-O_2 exposure comparing the semi-quantified concentrations of minerals present due to gas and temperature differences in weight percent (modified from Verba et al., 2012a)

Minerals	Pure CO_2 (50°C)	96% CO_2-4% O_2 (85°C)		96% CO_2-4% O_2 (50°C)	
	84 days	28 days	53 days	28 days	56 days
Portlandite $Ca(OH)_2$	24.2±4.2	10.5±1.8	11.2±2.1	19.5±1.2	12±2.1
Brownmillerite Ca_2FeAlO_5	8.8±1.5	8.3±1.2	8.3±1.8	12.4±1.8	5.3±0.9
Hatrurite Calcium Silicate Ca_3SiO_5	17±2.1	6.3±1.2	13.8±3.9	12.1±2.1	10±2.4
Larnite $Ca_2(SiO_4)$	16.6±4.8	13.4±3.9	13.5±3.9	9.5+0.3	2.7±1.5
Ettringite $Ca_6(Al(OH)_6)_2(SO_4)_3(H_2O)_{25.7}$	0	3.9±0.9	7.5±2.1	9.6±2.1	12±2.4
Hydrotalcite $Mg_6Al_2(CO_3)(OH)_{16}*4H_2O$	trace	2.3±0.9	2.3±1.2	4.2±1.2	3.5±0.9
Total $CaCO_3$ (Calcite, Vaterite, Aragonite)	22.5±3.9	54.6±3.3	54.2±1.9	26.7±1.2	23.2±2
Amorphous	1.9±0.9	0.6±0.3	2.2±4.2	6±0.3	30.7±4.2

Error = reported error x3, Materials Data Inc., Jade

Reexamination of the Class H Portland cement samples from Verba et al. (2012a) prior to strength tests in SEM showed that ettringite was not present in the carbonated exterior in contact with the acidic fluid, but rather was present in the adjacent zone in the cement paste. SEM analysis showed pores filled with ettringite needles with 0.5–3 µm-wide microfractures propagating toward the least resistant pathway around the mineral grains (Figure 3). These fractures are not interpreted as an artifact of sample preparation as this is a rough surface. Slow depressurization cannot be eliminated as a possible source of fractures. The presence of these fractures may compromise the cement integrity as they provide a pathway for acidic fluid to travel.

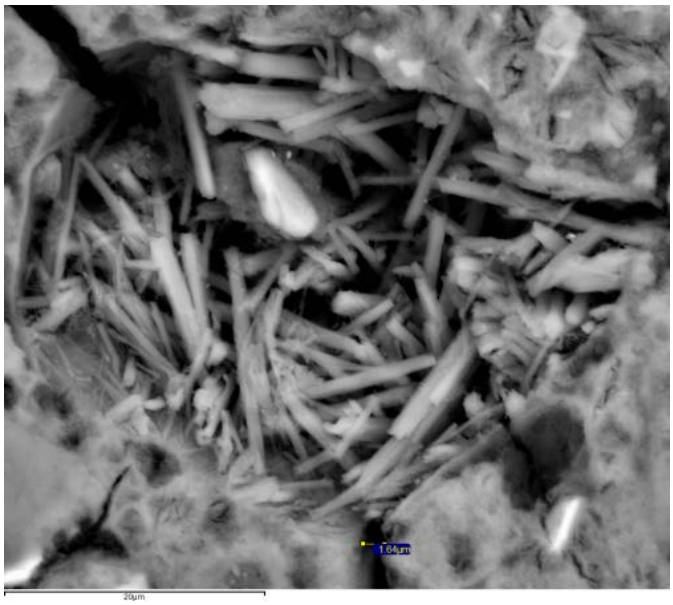

Figure 3: SEM backscatter electron (BSE) image. Close up of cement paste pore space filled with secondary ettringite needles with fractures after exposure to high P_{CO2-O2} and temperature. Scale bar is 20 µm.

3.2 ALTERATION FROM SULFURIC ACID

To study cement strength in contact with conventional sour gas stream (SO_2) or acid-waste stream in storage settings, cement was exposed to high pressure and temperature CO_2-O_2 for 28 days, followed by the injection a 7% (42 mL) sulfuric acid solution for an additional 7 days at atmospheric conditions. Figure 4 shows the cement paste after exposure to sulfuric acid with the precipitation of different sulfate minerals (gypsum, bassanite, and anhydrite) with electron microscopy and confirmed by wet preparation XRD analysis.

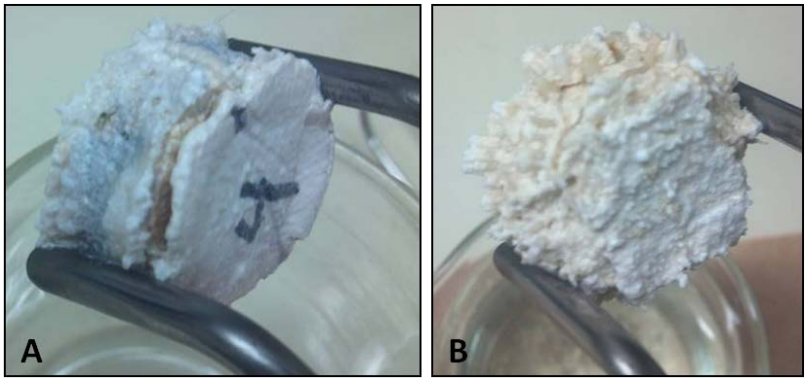

Figure 4: Alteration of hydrated Portland cement exposed to CO_2-O_2 under storage conditions for 28 days and then atmospheric conditions with 7% sulfuric acid for 7 days. A) Degradation of cement paste core cured with minor gypsum precipitation at 85°C. B) Crystalline precipitation of gypsum on Portland cement cured at 50°C.

Higher temperature was observed to increase the extent of alteration. The cement cured at 85°C and exposed to sulfuric acid resulted in spalled material, whereas cement cured at 50°C did not result in loss of cement. The cement cured at the higher temperature (85°C) lost 2 mm (4-mm diameter) on the sides of the cylinders and formed non-cohesive gypsum in the bottom of the glass beaker. Cement spalling is likely due to a higher hydration temperature, which resulted in a more crystalline C-S-H, such as tobermorite as determined with XRD analysis. Once combined with acidic fluids, and $Ca(OH)_2$ was replaced by calcite as seen in Figure 5, the adjacent zone began to lose calcium from the C-S-H structure.

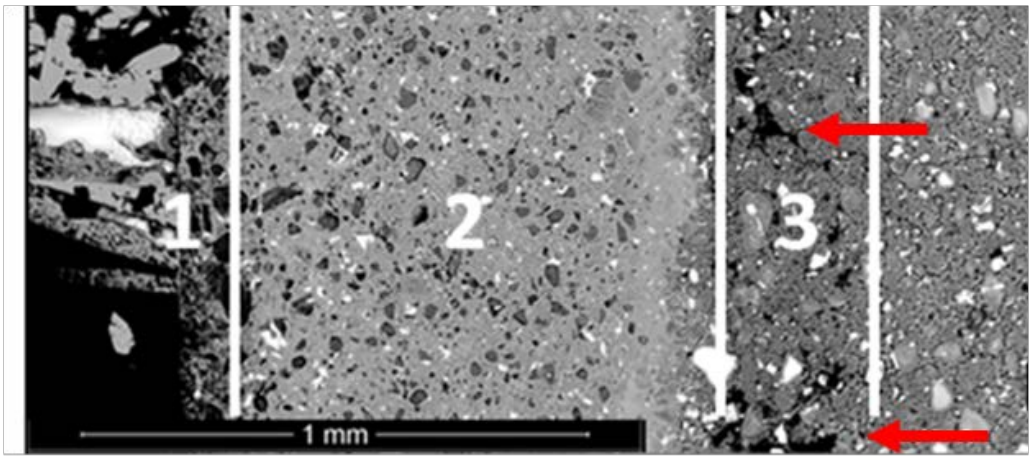

Figure 5: SEM BSE image of cement paste prior to exposure to sulfuric acid. Red arrows indicated the adjacent Zone 3 to the carbonated (Zone 2) where calcium has been leached. Zone 1 is the exterior of the sample in contact with acidic fluids.

Conversely, the cement sample exposed to the lower curing temperature (50°C) precipitated pure crystalline gypsum with a growth of ~4 mm in diameter and 5.5 mm in length (Figure 4B). It can be speculated that environmental factors such as temperature play an essential role in cement stability in co-storage setting. Lower temperatures allow the precipitation of expansive sulfate minerals. High hydration temperature and mixed gases may degrade the cement structure to the point it is completely unstable for storage purposes, as simulated with 7% H_2SO_4 cured at 85°C.

3.3 TENSILE POINT LOAD TESTS

Point load tests (Table 2) were performed on the following Portland cement samples cured for 28 days: 1) [10] in M(Ca-Mg-Na-Cl) brine Portland, but not exposed to any gases; 2) [6] exposed to CO_2; 3) [5] exposed to CO_2-O_2; and 4) [4] exposed to CO_2-O_2 and immersion in sulfuric acid. A marble sample, which is representative of natural cemented limestone that has undergone higher pressure and temperature conditions, was tested to compare its tensile strength to that of the hydrated cement; the tensile strength of the marble sample was 5.67 MPa.

Table 2: Point load test data to determine tensile strength of: 1) marble, cement paste cured in 1 M NaCl, $CaCl_2$, and $MgCl_2$, brine (no exposure to gas); 2) CO_2; 3) CO_2-O_2 exposed cement; and then 4) submerged in H_2SO_4. Nigel's Correction to equivalent Uniaxial Tensile Strength was used to standardize the point test.

Sample ID	Core Diameter (in)	Thickness (in)	Load (lbs) on Failure	K- Geometry factor	Tensile Strength (psi)	Nigels Correction	Average Tensile (psi)	(MPa)
Marble	0.98	0.58	504	1.18	1039	823	**653**	**5.67**
Brine (surrogate) cured cement pre-exposure								
1	1.03	0.47	310	1.53	977	774		
2	1.04	0.48	271	1.51	823	652		
3	1.04	0.43	271	1.69	1031	817		
4	1.02	0.46	279	1.56	938	743		
5	1.04	0.50	349	1.47	995	789	**752**	**5.18± .55**
6	1.03	0.44	295	1.62	1042	825		
7	0.98	0.47	319	1.47	1032	818		
8	1.03	0.43	194	1.67	728	577		
9	1.05	0.46	287	1.60	956	758		
10	1.02	0.52	372	1.38	964	764		
Brine (surrogate) cured cement CO_2 exposure								
1B	1.03	0.37	124	1.93	1008	799		
[1]2B	1.04	0.28	775	2.63	7122	5645		
3B	1.06	0.31	136	2.40	999	792	**840**	**5.79± 0.93**
4B	1.04	0.32	124	2.25	833	660		
5B	1.02	0.50	450	1.42	1247	988		
6B	1.03	0.48	399	1.50	1213	961		
Brine cured, CO_2-O_2 gas exposed								
1A	1.02	0.52	271	1.38	707	561		
2A	1.02	0.54	252	1.32	600	475		
3A	1.01	0.42	202	1.68	798	632	**600**	**4.14± .57**
4A	1.02	0.47	271	1.51	851	674		
5A	1.01	0.44	229	1.62	829	657		
Brine cured cement, CO_2-O_2 H_2SO_4 exposure								
1 (50°C)	1.06	0.50	343	1.49	971	770	**724**	**4.99± 0.45**
2 (50°C)	1.16	0.67	550	1.21	855	677		
3 (85°C)	1.21	0.70	504	1.21	711	563	**490**	**3.38± 0.71**
4 (85°C)	1.01	0.50	191	1.41	527	418		

[1]*Excluded from data (sample did not fail)*

The average tensile strength of the cement after curing in brine was 5.18 MPa, and the CO_2 exposed samples had an average tensile strength of 5.79 ±0.9 MPa (Table 2). The average tensile strength for samples exposed to CO_2-O_2 cured at 50°C was 4.14 ±0.57 MPa. The sulfuric acid leached samples averaged a tensile strength of 4.99 ±0.45 MPa at 50°C and 3.38 ±0.71 MPa at 85°C. The cement exposed to pure CO_2 gas had a slightly higher tensile strength than the unexposed (brine cured) samples by an average of 11.7%. The deviation in strength falls within the range of cured cement strength indicating that carbonation may or may not affect cement paste strength. The change in strength, if any, appears to be relatively small. Regardless, CO_2-O_2 samples exposed to mixed gas were weaker than both the unexposed and CO_2-exposed cement, as Figure 6 displays.

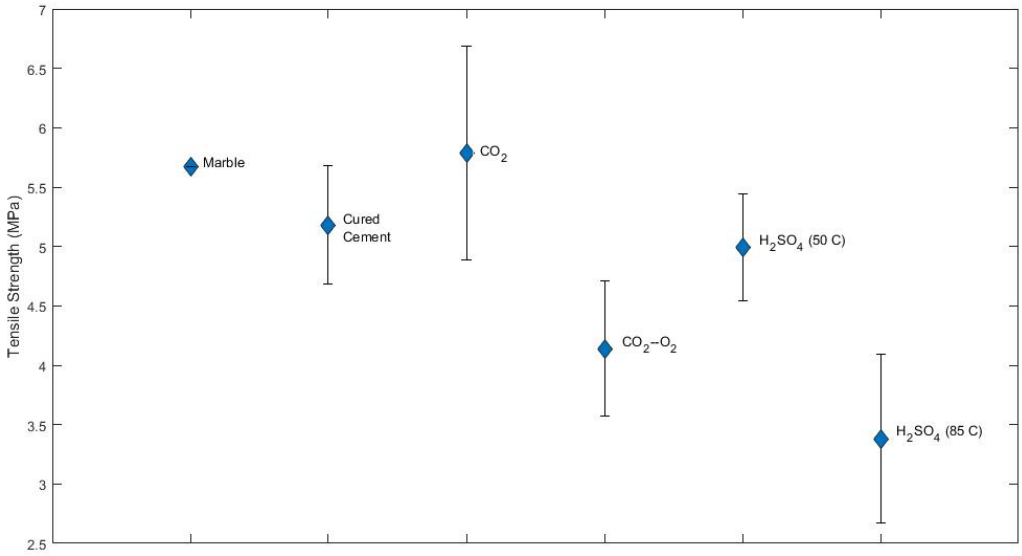

Figure 6: Average tensile strength for cured Portland cement samples exposed to CO_2; cured cement samples exposed to CO_2-O_2; CO_2-O_2 and sulfuric acid leach, and a marble sample used for high pressure and natural temperature. Error bars represent standard deviation.

These test results indicate that CO_2-O_2 may decrease the tensile strength of cement with a 95% confidence level. The cement paste strength decreased by 1 MPa (20% loss) at 50°C, which could be due to secondary ettringite precipitation and cement carbonation. As stated earlier, SEM analysis confirms that the presence of ettringite in all samples with CO_2-O_2 could play a role in decreased strength. Furthermore, SEM elemental mapping depicts the distribution of sulfur from gypsum bonded to the C-S-H prior to exposure to any gases. The sulfur appears to have acted as a nucleation site for the ettringite to precipitate after exposure to the oxygen gas.

Alternatively, cement paste exposed to CO_2-O_2 in the higher 85°C and then submerged in sulfuric acid displayed a ~2 MPa (34.7%) strength loss, on average for the two cases studied. This strength loss is likely due to both the influence of hydration temperature, as well as secondary mineral precipitation as seen in SEM analysis (Figure 3–5). However, the number of measurements taken (2) means that the difference in strengths between hydrated cement paste and cement paste exposed to H_2SO_4 cannot be distinguished with any statistical significance. At 50°C, the cement paste after H_2SO_4 immersion had a 3.7% loss compared to the hydrated cement

paste, which is well within the standard deviation of the unaltered hydrated cement paste. The addition of sulfur to the system after the exposure to CO_2-O_2 gas appears to have "maintained" the strength at lower temperatures. While the sample may have contained ettringite, the infilling of gypsum in pore space or fractures appears to have modified the tensile strength of the cement cylinder. The mechanical properties of gypsum may have contributed to the total strength of the cement at 50°C. Ambient tensile strength of gypsum has been reported in a range of 1.0–4.1 MPa (Clancy, 1999; Padevět et al., 2011). However, it is unclear if longer exposure, beyond 7 days, to sulfuric acid would impact the final strength at the lower temperature.

3.4 COMPRESSION TESTS

Compressive strength values for 28-day cured cement paste, CO_2-O_2-exposed, and CO_2-O_2-gas and sulfuric acid leach are presented Table 3 and Figure 7. Samples exposed to pure CO_2 were not analyzed for compressive strength because there were not enough samples to determine statistical significance. This study shows a clear reduction in the cement paste's compressive strength when subjected to high P_{CO2} co-stored gases as compared to that of unaltered hydrated cement.

Table 3: Compressive tests on hydrated Portland cement cured in a 1 M NaCl, $CaCl_2$, and $MgCl_2$, brine, then cement samples exposed to CO_2-O_2 at 50°C and 85°C, and then samples submerged in sulfuric acid at 50°C and 85°C.

Sample	Compressive Strength[1] (psi)	Compressive Strength (MPa)
Hydrated cement 1	4,720	32.54
Hydrated cement 2	4,872	33.59
Hydrated cement 3	4,817	33.21
Hydrated cement 4	5,420	37.37
CO_2-O_2 1 (50°C)	4,033	27.81
CO_2-O_2 2 (50°C)	4,226	29.14
CO_2-O_2 3 (85°C)	3,206	22.11
CO_2-O_2 4 (85°C)	3,676	25.34
H_2SO4 (50°C)	3,704	25.54
H_2SO4 (85°C)	2,946	20.31

[1]factored to cross sectional area

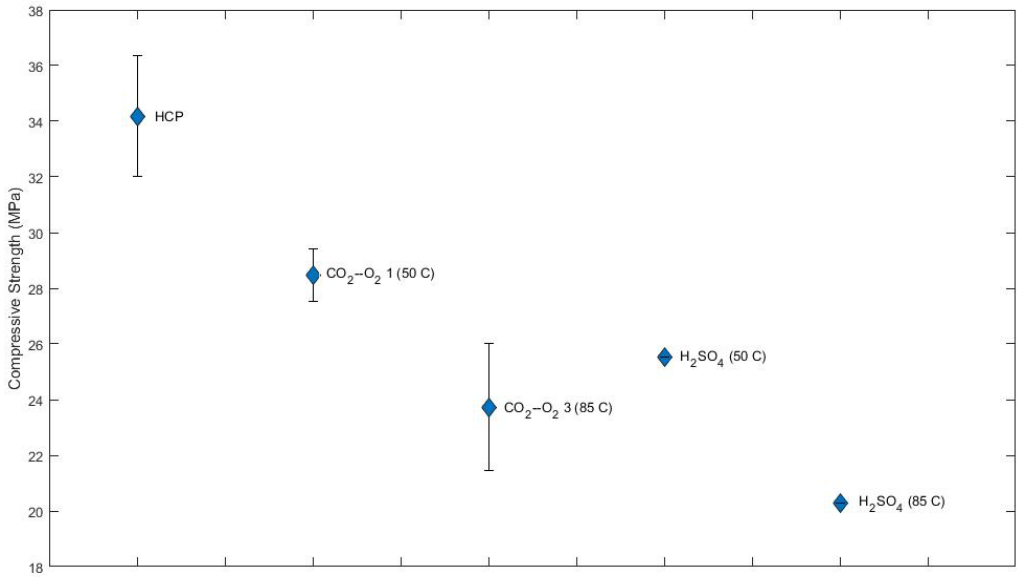

Figure 7: Compressive strength of cement samples comparing cured cement at 50°C, co-stored simulated, CO_2-O_2 mixed gas for 56 days at both 50°C and 85°C, and sulfuric acid submerged cement cured at both 50°C and 85°C.

All hydrated cement samples cured in 1 M mixed brine for 28 days had an average compressive strength of 34.18 ±2.17 MPa. In addition, petrography analysis showed that much of the paste remained unhydrated. In this study, all values for the hydrated cement paste were lower than those found by Kim et al. (1998) of 51.7 MPa at 40°C w/c=0.35 for 7 days and aged 28 days. However, the measurements do indicate moderate strength after curing as they exceed the minimum 20.7 MPa strength as defined by the Portland Cement Association (Kosmatka et al., 2002).

Initial compressive strength results indicate all cement samples after exposure to mixed gases deviate from the values of the cured cement paste. Cement paste samples exposed to only CO_2-O_2 mixed gas for 56 days at 50°C had an average compressive strength of 28.5±0.94 MPa at 50°C and 23.73±2.29 MPa at 85°C. After submersion in sulfuric acid, the cement showed reduced strength of 25.5 MPa at 50°C and 20.3 MPa at 85°C.

One significant observation was the influence of temperature on compressive strength. All cement samples cured at 85°C showed a clear reduction in compressive strength when immersed in acidic fluids. As stated earlier, it is evident by the results in this study that the physical development and chemical characteristics of the cement paste are dependent on the pressure and temperature conditions at which the cement is cured. Specifically, the high curing temperature increases the initial rate of hydration of the cement, and the C-S-H gel becomes more crystalline, compressive strength develops earlier, and ultimately lowers compressive strength (Nelson, 1990). These studies confirm that curing wellbore cement under high temperature (85°C) in-situ conditions results in a more crystalline C-S-H structure, leading to reduction of cement paste strength; the addition of the gases further exacerbated and weakened the cement cured.

It is also important to note that the present study examined only two samples under the influence of sulfuric acid, and therefore more experimental analysis is required to obtain results that are

statistically significant. These results showed that the cement paste sample with gypsum crystals cured at 50°C had a slightly higher compressive strength than that of the sample cured at 85°C. Cement samples exposed to CO_2-O_2 conditions and then submerged in sulfuric acid had a 10 to 15 MPa decrease in strength in comparison to the cured hydrated cement. It is inferred that the impact of the secondary minerals played a key role in the strength integrity. Furthermore, temperature appears to accelerate the loss of cement strength based on these initial tests.

4. CONCLUSIONS

This study sought to improve the understanding of the impact of co-storage on wellbore cement integrity, and to determine if secondary mineral precipitation influences the strength of cement paste. Pressure and temperature are shown to influence the hydration of cement, which is vital for cement strength and durability.

In this study, (co)-storage of CO_2, CO_2-O_2, and exposure to sulfuric acid precipitated secondary minerals, specifically calcium carbonate, ettringite or gypsum, which appears to generally impact the cement paste. While the tensile strength of cement increased slightly after exposure to CO_2, it is statistically insignificant indicating carbonation may have little impact on the cement. The addition of O_2 to the gas injection appears to have weakened the cement. This likely resulted from secondary development of ettringite and cement expansion. In addition, geochemical modeling predicts that the dissolution of SO_2 gas in formation water results in sulfuric acid, which reacts with the cement to form gypsum, and appears to weaken cement's compressive strength. Furthermore, the combination of higher temperature (85°C) during hydration and gas exposure appears to be damaging, evident by the material spalled during the test. However, it is important to note that sample strength measurements were conducted after the samples were removed from the reaction conditions to ambient temperature and pressure rather than under in situ confined conditions. To better gauge whether well cement exposed to CO_2 and co-storage gases can maintain its structural integrity and viability as a seal to unwanted fluid migration, further studies should be conducted to address their performance under confined conditions.

5. REFERENCES

API. *API Recommended Practice 10B. Recommended Practice for Testing Well Cements*; American Petroleum Institute: Washington, DC, 1997; p 133.

ASTM C 109, Test Method for Compressive Strength of Hydraulic Cement Mortars (Using 2-in or [50-mm] Cube Specimens). *Annu. Book ASTM Stand*. 1998, 04.01.

ASTM C 150, Standard Specification for Portland Cement. *Annu. Book ASTM Stand*. 2013, 04.01.

ASTM C 873, Test Method for Compressive Strength of Concrete Cylinders Cast in Place in Cylindrical Molds. *Annu. Book ASTM Stand*. 2013, 04.02.

Barron, A. *Application of Portland cement in the energy services industry*; Connexions Project; Rice University, Houston, TX, 2009.

Bachu, S.; Watson, T. L. Review of failures for wells used for CO_2 and acid gas injection in Alberta, Canada. *Energy Procedia* **2009,** *1*, 3531–3537.

Barlet-Gouedard, V.; Rimmele, G.; Porcherie, O.; Quisel, N.; Desroches, J. A. Solution against well cement degradation under CO_2 geological storage environment. *Int. J. Greenhouse Gas Control* **2009,** *3*, 206–216.

Bentur, A.; Berger, R. L.; Kung, J. H.; Milestone, N. B.; Young, J. F. Structural properties of calcium silicate pastes: II, Effect of curing temperature. *Journal of American Ceramic Society* **1979,** *62*, 362–366.

Bergman, P. D.; Winter, E. M. Disposal of carbon dioxide in the U.S. *Energy Conversion Mgmt.* **1995,** *36*, 523–526.

Bresson, B.; Zanni, H. Pressure and temperature influence on tricalcium silicate hydration. A 1H and 29Si NMR study. *J. Chim. Phys.* **1998,** *95*, 327–331.

Bresson, B.; Meducin, F.; Zanni, H. Hydration of tricalcium silicate (C_3S) at high temperature and high pressure. *Journal of Materials Science* **2002,** *37*, 5355–5365.

Bruant, R. G.; Guswa, A. J.; Celia, M. A.; Peters, C. A. Safe storage of CO_2 in deep saline aquifers. *Environ. Sci. Technology* **2002,** *36*, 240–245.

Carey, J. W.; Wigand, M.; Chipera, S. J.; Wolde Gabriel, G.; Pawar, R.; Lichtner, P. C.; Wehner, S. C.; Raines, M. A.; Guthrie, G. D. Analysis and performance of oil well cement with 30 years of CO_2 exposure from the SACROC unit, West Texas, U.S.A. *Int. J. Greenhouse Gas Control* **2007,** *1*, 75–85.

Clancy, P. Time and Probability of Timber Framed Walls in Fire, Ph.D. Thesis, Centre of Environmental Safety and Risk Engineering, Faculty of Engineering and Science, Victoria University of Technology, Victoria, Australia, 1999.

Chi, J. M.; Huang, R.; Yang, C. C. Effect of carbonation on mechanical properties of concrete using accelerated testing method. *J. Mar. Sci. Technol.* **2002,** *10*, 14–20.

Collepardi, M. A state-of-the-art review on delayed ettringite attack on concrete. *Cem. Concr. Compos.* **2003,** *25*, 401–407.

Collepardi, M. Damage by delayed ettringite formation. *Concr. Int.* **1999,** *21*, 69–74.

Crow, W.; Williams, B.; Carey, J. W.; Celia, M.; Gasda, S. Wellbore integrity analysis of a natural CO_2 producer. Proceedings of the 9th Int. Conf. Greenhouse Gas Control Technologies, Washington, DC, 2009.

DOE. Carbon Storage Atlas- Fifth Edition (Atlas 5); U.S. Department of Energy, National Energy Technology Laboratory. Pittsburgh, PA, 2015.

Diamond, S. Delayed Ettringite Formation, Processes and Problems. *Cem. Concr. Compos.* **1996,** *18*, 205–215.

Duguid, A.; Scherer, G. Degradation of oilwell cements due to exposure to carbonated brine. *Int. J. Greenhouse Gas Control* **2009,** *4*, 546–560.

Duguid, A.; Radonjic, M.; Scherer, G. Degradation of well cements exposed to carbonated brine. Proceedings from the 4th Annual Conference on Carbon Capture and Sequestration, at Monitor and Exchange Publications and Forum, Washington, DC, May 2–5, 2005.

Duguid, A.; Radonjic, M.; Scherer, G. W. Degradation of cement at the reservoir/cement interface from exposure to carbonated brine. *Int. J. Greenhouse Gas Control* **2011,** *5*, 1413–1428.

Fabbri, A.; Corvisier, J.; Schubnel, A.; Brunet, F.; Goffe, B.; Rimmele, G.; Barlet-Gouedard, V. Effect of carbonation on the hydro-mechanical properties of Portland cements. *Cem. Concr. Res.* **2009,** *39*, 1156–1163.

Famy, C.; Taylor, H. F. W. Ettringite in hydration of Portland cement concrete and its occurrence in mature concretes. *ACI Mater. J.* **2001,** *98*, 350–356.

Feldman, R. F.; Ramachandran, V. S. Character of Hydration of $3CaO•Al_2O_3$. *J. Amer. Cer. Soc* **1966,** *49*, 268–273.

Flatt, R.; Scherer, G. W. Thermodynamics of crystallization stresses in DEF. *Cem. Concr. Res.* **2008,** *38*, 325–336.

Fu, Y.; Beauidoin, J. J. Mechanism of delayed ettringite formation in Portland cement system. *ACI Mater J.* **1996,** 327–33.

Glasser, F. P. The role of $Ca(OH)_2$ in Portland cement concretes. In *Calcium Hydroxide in Concrete*; Skalny, J., Gebauer, J., Odler, I., Eds.; The American Ceramic Society: Westerville, OH, 2001; pp 11–36.

Glasser, F. P.; Marchand, J.; Samson, E. Durability of concrete: Degradation phenomena involving detrimental chemical reactions. *Cem. Concr. Res.* **2008,** *38*, 226–246.

Goodman, A.; Hakala, A.; Bromhal, G.; Deel, D.; Rodosta, T.; Frailey, S.; Small, M.; Allen, D.; Romanov, V.; Fazio, J.; Huerta, N.; McIntyre, D.; Kutchko, B.; Guthrie G. U.S. DOE methodology for development of geologic storage potential for carbon dioxide at national and regional scale. *Int. J. Greenh. Gas Control* **2011,** *5*, 952–965

Hangx, S.; van der Linden, A. No TitleDefining the Brittle Failure Envelopes of Individual Reaction Zones Observed in CO_2-Exposed Wellbore Cement. *Environ. Sci. Technol.* **2016,** *50*, 1031–1038.

Hewlett, P. C., Ed. Lea's Chemistry of Cement and Concrete, 4th ed.; Arnold: London, 1998, pp 299–342.

International Centre for Diffraction Data. Powder diffraction file update, PDF-2; 2008.

Jacquemet, N.; Pironon, J.; Saint-Marc, J. Mineralogical changes of a well cement in various H_2S-CO_2(-brine) fluids at high pressure and temperature. *Environ. Sci. Technol.* **2008,** *42*, 282–288.

Johannesson, B.; Utgenannt, P. Microstructural changes caused by carbonation of cement mortar. *Cem. Concr. Res.* **2001,** *31*, 925–931.

Johansen, V.; Thaulow, N.; Skalny, J. Simultaneous presence of alkali-silica gel and ettringite in concrete. *Cem. Concr. Res.* **1993,** *5*, 23–29.

Kim, J. K.; Moon, Y. H.; Eo, S. H. Compressive strength development of concrete with different curing time and temperature. *Cem. Concr. Res.* **1998,** *28*, 1761–1773.

Kosmatka, S. H.; Kerkhoff, B.; Panarese, W. C. Design and Control of Concrete Mixtures, EB001; Portland Cement Association, 2002; pp 372.

Kutchko, B. G.; Strazisar, B. R.; Dzombak, D. A.; Lowry, G. V.; Thaulow, N. Degradation of well cement by CO_2 under geologic sequestration conditions. *Environ. Sci. Technol.* **2007,** *13*, 4787–4792.

Kutchko, B. G.; Strazisar, B. R.; Huerta, N.; Lowry, G. V.; Dzombak, D. A.; Thaulow, N. CO_2 reaction with hydrated Class H well cement under geologic sequestration conditions: effects of flyash admixtures. *Environ. Sci. Technol.* **2009,** *43*, 3947–3952.

Kutchko, B. G.; Strazisar, B. R.; Lowry, G. V.; Dzombak, D. A.; Thaulow, N. Rate of CO2 attack on hydrated class H well cement under geologic sequestration conditions. *Environ. Sci. Technol.* **2008,** *42*, 6237–6242.

Kutchko, B.; Strazisar, B.; Hawthorn S.; Lopano, C.; Miller, D.; Hakala, A.; Guthrie, G. H_2S-CO_2 Reaction with Hydrated Class H Well Cement: Acid-Gas Injection and CO_2 Co-sequestration. *Environ. Sci. Technol.* **2011,** *5*, 880–888.

Le Saout, G.; Lécolier, E.; Rivereau, A.; Zanni, H. Chemical structure of cement aged at normal and elevated temperatures and pressures. Part I. Class G oilwell cement. *Cem. Concr. Res.* **2013**.

Le Saout, G.; Lécolier, E.; Rivereau, A.; Zanni, H. Study of oilwell cements by solid-state NMR. *C.R. Chimie* **2004,** *7*, 383–388.

Lécolier, E.; Rivereau, A.; Ferrer, N.; Audibert, A.; Longaygue, X. Durability of oilwell cement formulations aged in H_2S-containing fluids. IADC/SPE Drilling Conference, Miami, FL, Feb 21–23, 2006; IADC/SPE 99105.

Logan, J. M.; Hastedt, M.; Lehnert, D.; Denton, M. A case study of the properties of marble as a building veneer. *Int. J. Rock Mech. Mm Sci. & Geomech Abstr.* **1993,** *30*, 1531–1537.

Meller, N.; Hall, C.; Jupe, A. C.; Colston, S. L.; Jacques, S. D. M.; Barnes, P.; Phipps, J. The paste hydration of brownmillerite with and without gypsum: a time resolved synchrotron diffraction study at 30, 70, 100, and 150°C. *J. Mater. Chem.* **2004,** *14*, 428–435.

Mehta, P.; Monteiro, P. *Concrete: Microstructure, properties, and materials*, 3rd ed.; McGraw Hill, 2006.

Moroni, N.; Repetto, C.; Ravi, K. Zonal isolation in reservoir containing CO_2 and H_2S. In IADC SPE Drilling Conference, 2008; IADC/SPE112703.

NATCARB Database. NatCarb, 2013 version. http://www.natcarb.org.

Nelson, E. B. *Well cementing*; Schlumberger Educational Services: Sugar Land, TX, 1990.

Padevět, P.; Tesárek, P.; Plachý, T. Evolution of mechanical properties of gypsum in time. *Int J Mech* **2011,** *5*, 1–9.

Palandri, J. L.; Kharaka, Y. K. Ferric Iron-Bearing Sediments as a Mineral Trap for CO_2 Sequestration: Iron Reduction using Sulfur-Bearing Waste Gas. *Chemical Geology* **2005,** *217*, 351–364.

Reed, M.; Palandri, J. SOLTHERM.H08, A Database of Equilibrium Constants for Minerals and Aqueous Species; University of Oregon, Eugene, OR, 2013.

Rimmelé, G.; Barlet-Gouédard, V.; Porcherie, O.; Goffé, B.; Brunet, F. Heterogeneous porosity distribution in Portland cement exposed to CO_2-rich fluids. *Cem. Concr. Res.* **2008,** *38*, 1038–1048.

Scherer, G. W. Stress from crystallization of salt. *Cem. Concr. Res.* **2004,** *34*, 1613–24.

Scherer, G. W.; Kutchko, B.; Thaulow, N.; Duguid, A.; Mook, B. Characterization of cement from a well at Teapot Dome Oil Field: Implications for geologic sequestration. *Int. J. Greenhouse Gas Control* **2011,** *5*, 115–1240.

Scherer, G. W.; Zhang, J.; Weissinger, E. A.; Peethamparan, S. Early hydration and setting of oil well cement. *Cement Concr. Res.* **2010,** *40*, 1023–1033.

Shen, J. C. Effects of CO_2 attack on cement in high-temperature applications. SPE/IADC Drilling Conference, New Orleans, LA, Feb 28–Mar 3, 1989; SPE 18618.

Stark, J.; Bollmann, K. Ettringite formation in concrete pavements. ACI Spring Convention, Seattle, WA, 1997; Special Publication ACI Journal, 1999.

Taylor, H. F. W. *Cement chemistry*; Academic Press: New York, 1997.

Taylor, H. F. W. Symposium on Materials Science of Cement and Concrete, High Tatra, Slovakia, June 1993.

Taylor, H. F. W.; Famy, C.; Scrivener, K. L. Delayed ettringite formation. *Cem. Concr. Res.* **2001,** *31*, 683–693.

Thaulow, N.; Lee, R. J.; Wagner, K.; Sahu, S. Effect of calcium hydroxide on the form, extent, and significance of carbonation. In *Calcium Hydroxide in Concrete*; Skalny, J., Gebauer, J., Odler, I., Eds.; The American Ceramic Society: Westerville, OH, 2001; pp 191–201.

Um, W., & Rod, K. Geochemical alteration of wellbore cement by CO_2 or CO_2 + H_2S reaction during long-term carbon storage. *Greenhouse Gasses* **2016,** *1595*.

Walsh, S. D. C.; Mason, H. E.; Du Frane, W. L.; Carroll, S. A. Mechanical and hydraulic coupling in cement-caprock interfaces exposed to carbonated brine. *Int. J. Greenhouse Gas Control* **2014,** *25*, 109–120. doi.org/10.1016/j.ijggc.2014.04.001

Verba, C. A.; O'Connor, W. K.; Rush, G. E. CO_2 alteration rates for class H Portland cement. Presented at 9th Annual Conference on Carbon Capture and Sequestration, Pittsburgh, PA, May 10–13, 2010.

Verba, C. A.; O'Connor, W. K.; Rush, G. E. Implications of geologic CO_2 sequestration for basaltic and siliceous host rocks and class H cement. Presented at 10th Annual Carbon Sequestration Conference, Pittsburgh, PA, May 2–5, 2011.

Verba, C. A.; O'Connor, W.; Ideker, J. Advances in Geological CO_2 Sequestration and Co-Sequestration with O_2. ACI-CANMET Special Publication in Recent Advances in Concrete Technology and Sustainability Issues. Prague, Czech Republic, 2012a; Special Publication V 298, pp. 1–16.

Verba, C. A.; Kutchko, B.; Reed, M. H. Co-Sequestration Geochemical Modeling: Simple Brine Solution + CO_2-O_2-SO_2. American Geophysical Union, Fall Meeting 2012, 2012b; Abstract H23A-1313.

Zhang, M.; Bachu, S. Review of integrity of existing wells in relation to CO_2 geological storage: What do we know? *Int. J. Greenhouse Gas Control* **2011,** *5*, 829–840.

Zhang, J.; Weissinger, E. A.; Peethamparan, S.; Scherer, G. W. Early hydration and setting of oil well cements. *Cem. Concr. Res.* **2010,** *40*, 1023–1033

APPENDIX: CHIM-XPT GEOCHEMICAL MODELING

Summary: Surrogate Brine Solution + gas phases 95.5% CO_2 + 4% O_2 + 1.5% SO_2

To simulate CO_2-O_2-SO_2 gas immersion experiments, a set amount of initial gas mixture (95.5% CO_2, 1.5 SO_2 and 4% O_2) was added to a specific volume of surrogate brine and Class H Portland cement, in this experiment at simulated downhole expected conditions were 50°C and 28.6 MPa. The initial surrogate brine composition consisted of 0.16 mole/L $CaCl_2$, 0.02 mole/l $MgCl_2$, and 0.82 mole/L NaCl.

The geochemical model CHIM-XPT had the capability to reach a gas saturation ~23 MPa before the program failed to converge. The expected content should be similar as it will not significantly change to the expected pressure of 28.6 MPa.

The final molality of SO_3^{2-} is $0.64665E^{-02}$; $CaSO_4$ (aq) is $0.30199E^{-02}$; HSO_4- is $0.11819E^{-04}$. The total sulfate molality is 0.0095 M. A one normal (1 N) sulfuric acid solution is ~1 m in sulfate and ~2 m in hydrogen ion (as normality is "per liter of solution," not per kg of solvent water). One could calculate that in a 600 mL liquid volume (given experimental volume) would result in a 0.0095 m sulfate solution [0.6 L x .0095 moles of sulfate = 0.0057 moles of sulfate]. Given that for a 1 N acid concentration of sulfuric acid, 1 mL contains 0.001 mole of sulfate [0.0057/.001 = 5.7 mL] there is an expected amount of 5.7 mL of 1 N sulfuric acid to make the desired sulfate concentration in 600 mL of solution.

Based on the geochemical modeling, there is a final excess of 31% O_2; this excess oxygen indicates that all H_2S from SO_2 disporportionation is oxidized to sulfate, thus no H_2S needs to be added to the sulfuric acid or gas mixture. The calculation shows that the gaseous SO_2 has a total mole fraction of 10^{-46}, which implies there would be no SO_2 remaining in the experimental head space. Any additional injection of SO_2 gas in the headspace would resupply sulfur ions to react with the solution and the cement at these conditions. The expected pH of the solution at experimental condition is 4.34, which would initiate a range of reactions as the system equilibrates. Figure A1 displays the change in pH and the precipitation of brucite ($Mg(OH)_2$) that is first replaced by calcite ($CaCO_3$), and then replaced by gypsum ($CaSO_4$*$2H_2O$). Furthermore, the geochemical model indicates additional reactions with sulfuric acid would likely precipitate additional gypsum and stable forms of anhydrite, stable form of calcite, and/or dolomite. Based on the geochemical modeling, the final gas composition consists of 67% CO_2-31%O_2 (minus 2% H_2O vapor), which can be added to the pressure vessel with 5.7 mL of sulfuric acid to simulate the desired conditions of co-stored gases.

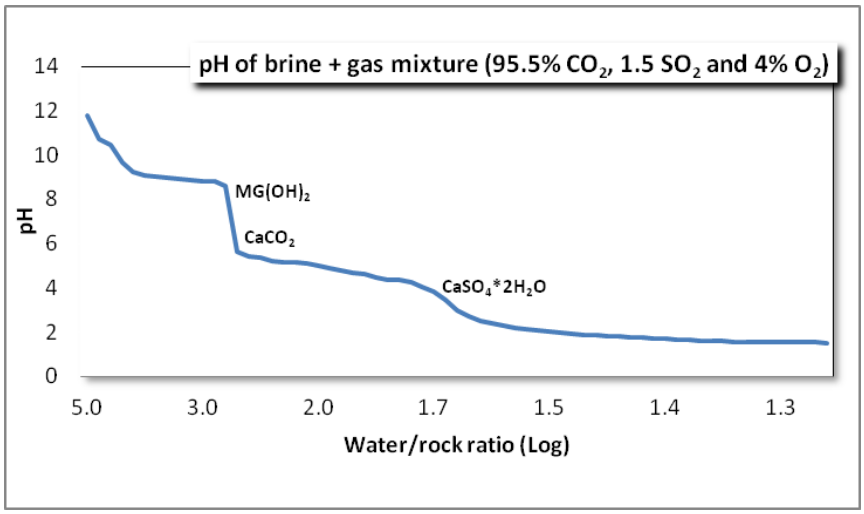

Figure A1: At simulated downhole expected conditions of 50°C and 28.6 MPa with the surrogate brine reacted with a gas mixture of 95.5% CO_2, 1.5 SO_2 and 4% O_2. As the reactant is consumed, the pH decreases, Brucite precipitates and is initially stable, dissolving at pH= 8.79 whereby calcite precipitates until dissolution at pH 5.10, and finally gypsum precipitates at a pH of 4.34 and is stable to a pH of 1.82.

Geochemical Model: CHIM-XPT Output File

The geochemical model CHIM-XPT uses text input files that are based on partial equilibrations using Formula Translating System (Fortran) to program computational fluid mineral equilibria. CHIM-XPT was utilized as it can distinguish saturation indices of carbonate minerals and cementitious minerals (Reed and Palandri, 2013). The geochemical system attempts to come into equilibrium in steps that can reach a loop limit and fail to converge, or reach equilibrium within the given data parameters. The loop is the maximum allowed number of Newton-Raphson iterations in the convergence calculation. If the system fails to converge, all aqueous species, gases, and minerals at the set temperature, pressure, or total liquid water have not summed to reach equilibrium. In this run of mixed gases, brine, and cement, the gas composition reached saturation at 25 iterations (25 loops), reaching a maximum of 23 MPa gas saturation. Due to the high chloride content, the geochemical reaction had to include a charge balance for all species of $1.1x10^{1}$. The details for the input data for CHIM-XPT are listed below in Tables A1–A4. The titration for added reactants (cement) is 0.01 g, which resulted in 40.6399 g reactant consumed within 1035.4 g of solution. This gave a water/rock ratio of 25.48 (log=-1.4062). There were no solid products that replaced original rock value.

Table A1: Input data of the initial composition of reactance gas in weight percent of 95.5% CO_2, 1.5 SO_2 and 4% O_2 reacting with cement in surrogate brine at 50°C and 28.6 MPa to accommodate ionic strength and ionic charge balance with chloride.

Initial Composition of Reactant Gas (wt%):
CO_2 gas 95.50 SO_2 gas 1.500
O_2 gas 4.000 0.000
[The CHIM results at 230.7 are not valid for gas properties; use 230.0389.]
Temperature = 50.00 C
Pressure = 28.6 MPa
Water: Moles liquid = 0.5453E+02 kg liquid = 0.9824E+00
Moles total = 0.5369E+02 kg total = 0.9673E+00 Activity = 0.9661
Stoichiometric ionic strength =0 .1632332E+01
True ionic strength =0 .1049589E+01
Chg. balance for total moles = -0.8601E-05 Max. difference allowed = 0.9183E-04

Table A2: Output file displaying the chemical species, their respective molality, activity, and activity coefficient of cement reacting with surrogate brine in a gas saturation of 95.5% CO_2, 1.5% SO_2 and 4% O_2 at 50°C and 28.6 MPa.

	Species (n)	Molality	Log Molality	Activity	Log Activity	Gamma	Log Gamma
1	H+	6.27E-05	-4.2026	4.48E-05	4.3484	7.15E-01	-0.1459
2	H_2O			9.66E-01	-0.0150	9.66E-01	-0.0150
3	Cl-	8.75E-01	-0.0580	5.80E-01	-0.2367	6.63E-01	-0.1786
4	SO4--	6.47E-03	-2.1893	1.05E-03	-2.9793	1.62E-01	-0.7900
5	HCO_3-	2.04E-02	-1.6901	1.32E-02	-1.8785	6.48E-01	-0.1884
6	HS-	5.81E-132	-131.2357	3.84E-132	-131.4156	6.61E-01	-0.1799
7	Ca++	1.19E-01	-0.9234	1.91E-02	-1.7181	1.60E-01	-0.7948
8	Mg++	1.55E-02	-1.8100	2.60E-03	-2.5852	1.68E-01	-0.7752
9	Na+	6.20E-01	-0.2076	4.04E-01	-0.3938	6.51E-01	-0.1861
10	Sr++	2.01E-05	-4.6967	3.19E-06	-5.4968	1.58E-01	-0.8001
16	CO_2,aq	8.52E-01	-0.0695	8.61E-01	-0.0651	1.01E+00	0.0044
17	CO_3-2	1.70E-07	-6.7693	2.79E-08	-7.5540	1.64E-01	-0.7847
18	CaCO3,aq	1.83E-06	-5.7385	1.83E-06	-5.7385	1.00E+00	0.0000
19	Ca(HCO_3)+	4.84E-03	-2.3155	3.08E-03	-2.5115	6.37E-01	-0.1960
20	CaCl+	1.13E-02	-1.9464	7.20E-03	-2.1425	6.37E-01	-0.1960
21	$CaCl_2$,aq	1.19E-03	-2.9232	1.19E-03	-2.9232	1.00E+00	0.0000
22	CaOH+	9.92E-10	-9.0033	6.32E-10	-9.1994	6.37E-01	-0.1960
23	$CaSO_4$,aq	3.02E-03	-2.5200	3.02E-03	-2.5200	1.00E+00	0.0000
24	HCl,aq	5.09E-06	-5.2931	5.09E-06	-5.2931	1.00E+00	0.0000
25	HClO,aq	8.51E-13	-12.0703	8.51E-13	-12.0703	1.00E+00	0.0000
26	ClO-	1.57E-15	-14.8044	1.04E-15	-14.983	6.63E-01	-0.1786
29	$MgCO_3$,aq	8.84E-08	-7.0533	8.84E-08	-7.0533	1.00E+00	0.0000
30	Mg(HCO_3)+	6.55E-04	-3.1836	4.17E-04	-3.3796	6.37E-01	-0.1960
31	MgCl+	1.86E-03	-2.7297	1.19E-03	-2.9257	6.37E-01	-0.1960
32	MgOH+	1.27E-09	-8.8976	8.06E-10	-9.0937	6.37E-01	-0.1960
33	NaCl,aq	4.43E-02	-1.3540	4.43E-02	-1.3540	1.00E+00	0.0000
34	NaOH,aq	3.46E-10	-9.4604	3.46E-10	-9.4604	1.00E+00	0.0000
35	O_2,aq	4.58E-02	-1.3388	4.63E-02	-1.3343	1.01E+00	0.0044
36	OH-	2.07E-09	-8.6849	1.45E-09	-8.8373	7.04E-01	-0.1525
38	H_2O_2,aq	1.08E-16	-15.9653	1.08E-16	-15.9653	1.00E+00	0.0000
47	HSO4-	1.18E-05	-4.9274	7.56E-06	-5.1213	6.40E-01	-0.1939
61	$SrCO_3$,aq	1.14E-10	-9.9422	1.14E-10	-9.9422	1.00E+00	0.0000
62	Sr(HCO_3)+	2.20E-06	-5.6581	1.40E-06	-5.8542	6.37E-01	-0.1960
63	SrCl+	2.10E-06	-5.6782	1.34E-06	-5.8743	6.37E-01	-0.1960
64	SrOH+	6.46E-14	-13.1899	4.11E-14	-13.3859	6.37E-01	-0.1960

Table A2 displays the molar concentrations of species after the reaction of the brine with the gas mixture; the most critical species is the total SO_4= $0.9498E^{-2}$ (molality) is equivalent to 0.0095 m. It can be extrapolated that all sulfate from the injection of SO_2 will result in the precipitation of crystallized gypsum; this gypsum may be stable in experimental conditions, specifically if the brine provides enough calcium cations for reaction and furthermore by any reaction with the presence of Class H cement. The SO_2 gas conversion is to mineral form, which indicates there is no risk of H_2S forming as verified by the remaining gas mixture as seen in Tables A3 and A4.

Table A3: The gas composition after cement paste has reacted with surrogate brine 95.5% CO_2, 1.5% SO_2 and 4% O_2 at 50°C and 28.6 MPa. The gas composition given here (CO_2-O_2 (minus the vaporous H_2O)) is the composition to mix with the liquid to simulate the desired experimental conditions.

Gas	Mole Fraction	phi	Fugacity	Partial P(bar)
H_2O,gas	2.10E-02	0.0297	1.43E-01	4.83E+00
CO_2,gas	6.70E-01	0.4163	6.42E+01	1.54E+02
CH_4,gas	3.26E-136	1.3588	1.02E-133	7.50E-134
H_2,gas	1.12E-41	1.1504	2.96E-39	2.57E-39
H_2S,gas	2.30E-130	0.3493	1.85E-128	5.30E-128
CO,gas	2.01E-43	1.0000	4.61E-41	4.61E-41
SO_2,gas	1.80E-47	1.0000	4.13E-45	4.13E-45
S_2,gas	7.86E-205	1.0000	1.80E-202	1.80E-202
SO_3,gas	1.74E-35	1.0000	4.00E-33	4.00E-33
O_2,gas	3.09E-01	1.0000	7.10E+01	7.10E+01

Table A4: The following gases and minerals are presently excluded from the matrix. This includes the saturation or likelihood of precipitation of mineral and presence of gases. If log Q/K< 0, the reaction or precipitation has yet to reach saturation. If log Q/K = 0, the reaction is at equilibrium. If log Q/K > 0 than the phase has reached saturation and exists as a free phase. Gases and minerals with log(Q/K) less than -5 are not listed below. Log fugacity is only relevant to gaseous species in pressures to determine the chemical equilibrium.

Gas or Mineral	Log K	Log Q	Log(Q/K)	Log(Q/K)/S	Affinity	Log Fugacity
H_2O, gas	3.29	-0.01	-3.3	-3.3	4.88E+03	-0.844
CO_2, gas	-5.56	-6.21	-0.65	-0.216	9.60E+02	1.807
CH_4, gas	5.12	-130.33	-135.45	-33.862	2.00E+05	-132.992
H_2, gas	9.95	-31.04	-40.99	-23.42	6.06E+04	-38.529
H_2S, gas	-5.57	-135.76	-130.19	-65.095	1.93E+05	-127.733
CO, gas	5.56	-37.23	-42.79	-13.167	6.33E+04	-40.336
SO_2, gas	4.16	-42.68	-46.84	-12.491	6.93E+04	-44.384
S_2, gas	-5.25	-209.45	-204.2	-31.415	3.02E+05	-201.743
SO_3, gas	23.19	-11.66	-34.85	-8.714	5.15E+04	-32.398
O_2, gas	62.65	62.04	-0.6	-0.403	8.94E+02	1.852
Anhydrite	-4.4	-4.7	-0.3	-0.15	4.45E+02	-
Aragonite	1.71	0.75	-0.95	-0.318	1.41E+03	-
Calcite	1.58	0.75	-0.83	-0.276	1.22E+03	-
Celestite	-5.61	-8.48	-2.87	-1.435	4.25E+03	-
Dolomite, ord	2.56	0.64	-1.93	-0.321	2.85E+03	-
Dolomite, dis	3.28	0.64	-2.64	-0.44	3.90E+03	-
Gypsum	-4.47	-4.73	-0.26	-0.065	3.87E+02	-
Halite	1.66	-0.63	-2.29	-1.144	3.38E+03	-
Magnesite	1.78	-0.12	-1.9	-0.632	2.80E+03	-
Strontianite	-0.3	-3.03	-2.73	-0.91	4.04E+03	-

NRAP is an initiative within DOE's Office of Fossil Energy and is led by the National Energy Technology Laboratory (NETL). It is a multi-national-lab effort that leverages broad technical capabilities across the DOE complex to develop an integrated science base that can be applied to risk assessment for long-term storage of carbon dioxide (CO_2). NRAP involves five DOE national laboratories: NETL, Lawrence Berkeley National Laboratory (LBNL), Lawrence Livermore National Laboratory (LLNL), Los Alamos National Laboratory (LANL), and Pacific Northwest National Laboratory (PNNL).

Technical Leadership Team

Diana Bacon
Lead, Groundwater Protection Working Group
Pacific Northwest National Laboratory
Richmond, WA

Jens Birkholzer
LBNL Lab Lead
Lawrence Berkeley National Laboratory
Berkeley, CA

Grant Bromhal
Technical Director, NRAP
Research and Innovation Center
National Energy Technology Laboratory
Morgantown, WV

Chris Brown
PNNL Lab Lead
Pacific Northwest National Laboratory
Richmond, WA

Susan Carroll
LLNL Lab Lead
Lawrence Livermore National Laboratory
Livermore, CA

Abdullah Cihan
Lead, Reservoir Performance Working Group
Lawrence Berkeley National Laboratory
Berkeley, CA

Tom Daley
Lead, Strategic Monitoring Working Group
Lawrence Berkeley National Laboratory
Berkeley, CA

Robert Dilmore
NETL Lab Lead
Research and Innovation Center
National Energy Technology Laboratory
Pittsburgh, PA

Nik Huerta
Lead, Migration Pathways Working Group
Research and Innovation Center
National Energy Technology Laboratory
Albany, OR

Rajesh Pawar
LANL Lab Lead
Lead, Systems/Risk Modeling Working Group
Los Alamos National Laboratory
Los Alamos, NM

Tom Richard
Deputy Technical Director, NRAP
The Pennsylvania State University
State College, PA

Josh White
Lead, Induced Seismicity Working Group
Lawrence Livermore National Laboratory
Livermore, CA

Sean Plasynski
Executive Director
Technology Development and
Integration Center
National Energy Technology Laboratory
U.S. Department of Energy

Heather Quedenfeld
Associate Director
Coal Development and Integration
National Energy Technology Laboratory
U.S. Department of Energy

Traci Rodosta
Technology Manager
Strategic Planning
Science and Technology Strategic Plans
and Programs
National Energy Technology Laboratory
U.S. Department of Energy

Darin Damiani
Program Manager
Carbon Storage
Office of Fossil Energy
U.S. Department of Energy

NRAP Technical Report Series